Pharmaceutical Sciences Asia

Pharm Sci Asia 2026; 53(2), 179-194

DOI:10.29090/psa.2026.02.26.9351

Research Article

A Chou-Talalay synergy framework reveals dose-sparing analgesic, antipyretic and anti-inflammatory effects of *Melastoma malabathricum* leaf extract combined with nanocurcumin in mice

Thi Phuong Nhung Tran*, Hong Quan Bui, Huyen Trang Luu, Ngoc Thuan Nguyen, Thi Truc Ly Le, Hoa Hong Chau Truong

Institute of Biotechnology - Food, Industrial University of Ho Chi Minh City, Ho Chi Minh City, 70000, Vietnam

ABSTRACT

Pain, inflammation, and fever share overlapping mediator networks, supporting dose-sparing, multi-target combinations. We evaluated a standardized *Melastoma malabathricum* leaf extract (ME) combined with nanocurcumin (NC) using Chou-Talalay quantitative synergy analysis and multi-model *in vivo* validation. ME and NC were quality-controlled by chromatographic fingerprinting and physicochemical characterization. In LPS-stimulated RAW 264.7 macrophages, single-agent and fixed-ratio combination dose-response relationships were modeled by median-effect analysis to compute combination index (CI) and dose-reduction index (DRI). For *in vivo* validation, Swiss albino mice were randomized into five groups per model: (i) vehicle control, (ii) model-matched positive control (tramadol, meloxicam, or paracetamol), (iii) ME alone (200 mg/kg), (iv) NC alone (50 mg/kg), and (v) ME+NC combination. Efficacy was assessed using hot-plate and formalin nociception, carrageenan-induced paw edema, and Brewer's yeast-induced pyrexia, with reference drugs to confirm assay sensitivity. ME+NC showed consistent synergism across effect levels (Fa 0.50-0.90), with CI 0.62-0.79 at Fa 0.50-0.75 and 0.58 at Fa 0.90, corresponding to practical dose-sparing (DRI ≈ 2.2-2.6 for ME and 2.7-3.1 for NC). *In vivo*, the combination produced the greatest improvements across pain, inflammation, and fever models versus either monotherapy, alongside larger reductions in pro-inflammatory cytokines and COX-2/iNOS and favorable shifts in oxidative stress markers, and was well tolerated under the study conditions, without evidence of overt short-term toxicity. Overall, ME+NC is a quality-controlled, CI/DRI-defined synergistic combination with coherent multi-symptom efficacy, warranting pharmacokinetic–pharmacodynamic optimization and evaluation in longer-term disease settings.

Keywords:
Melastoma malabathricum; Nanocurcumin; Chou-Talalay; Synergy; Dose-sparing; Analgesic

1. INTRODUCTION

Pain, inflammation, and fever frequently co-occur in clinical practice and reflect interlinked phenotypes driven by coordinated host-response networks rather than fully separable symptoms.[1] Although conventional symptomatic therapies (analgesics, antipyretics, and nonsteroidal anti-inflammatory drugs; NSAIDs) are effective, long-term or high-dose use is constrained by dose-dependent adverse events, including gastrointestinal injury, cardiovascular risk, and renal toxicity.[2] These limitations motivate dose-sparing strategies that preserve efficacy while lowering exposure to any single agent and, consequently, improving the overall therapeutic index. A mechanistic rationale for dose-sparing combinations lies in the interplay of mediators regulating pain, inflammation, and fever. Pro-inflammatory cytokines such as tumor necrosis factor-α (TNF-α), interleukin-1β (IL-1β),

***Corresponding author:**
* Thi Phương Nhung Tran Email: tranthiphuongnhung@iuh.edu.vn

and interleukin-6 (IL-6) activate downstream programs involving cyclooxygenase-2 (COX-2)-dependent prostaglandin synthesis, particularly prostaglandin E_2 (PGE_2), and inducible nitric oxide synthase (iNOS)-mediated nitric oxide signaling.[3] Collectively, these pathways amplify inflammatory cascades, promote peripheral and central sensitization, and contribute to hyperalgesia.[3] Oxidative stress and reactive oxygen species (ROS) further sustain cytokine signaling and reinforce feed-forward loops that perpetuate mediator release and nociceptive sensitization. Fever similarly arises from cytokine-triggered COX-2/PGE_2 signaling within thermoregulatory centers. Accordingly, targeting multiple nodes within the shared cytokine-COX-2/PGE_2-iNOS/NO-ROS axis provides broader and more dose-efficient control of these symptoms than single-target approaches.[4]

Botanical preparations are a rich source of multi-target bioactivity relevant to this mediator network. *Melastoma malabathricum* L. (hereafter, *M. malabathricum*) has long been used in ethnomedicine for inflammatory and pain-related conditions, and experimental studies report antinociceptive, anti-inflammatory, and antipyretic effects of leaf preparations in standard preclinical models, including hot-plate, formalin, carrageenan-induced paw edema, and yeast-induced pyrexia tests.[5] Although previous studies have characterized the individual pharmacological effects of *M. malabathricum* leaf preparations, no prior work has quantified their interaction with nanocurcumin using a formal CI/DRI synergy framework or validated the resulting dose-sparing combination across multiple *in vivo* symptom models within a single QC-anchored experimental pipeline. Phytochemical analyses further indicate that *M. malabathricum* leaves are enriched in polyphenolic constituents, including flavonoids and tannin-like compounds, which are commonly associated with antioxidant and immunomodulatory effects that can attenuate cytokine signaling and oxidative amplification loops.[6] However, reproducibility and translational confidence for botanicals can be compromised by variability in plant material related to geographic origin, seasonality, and extraction conditions. Therefore, rigorous botanical authentication and chemical standardization, supported by chromatographic fingerprinting, are increasingly required to ensure batch-to-batch consistency and interpretability when botanical extracts are evaluated as defined therapeutic entities.

Curcumin offers a complementary anti-inflammatory and antioxidant profile that intersects directly with the cytokine-COX-2/iNOS-ROS network but is limited *in vivo* by poor aqueous solubility, restricted absorption, and rapid metabolism, leading to variable systemic exposure and inconsistent therapeutic outcomes.[7] Nano-enabled curcumin formulations seek to address these limitations by improving dispersion and solubility, protecting curcumin from degradation, and enabling controlled release to enhance bioavailability and tissue distribution.[8] Nonetheless, performance claims should be supported by rigorous physicochemical characterization, including particle size distribution, polydispersity index, surface charge, encapsulation efficiency, drug loading, and release kinetics, to establish formulation consistency and biological credibility. Among nano-enabled platforms, poly(lactic-co-glycolic acid) (PLGA)-based nanoparticles are particularly attractive owing to their well-established biocompatibility, biodegradability, and capacity for sustained drug release; PLGA-curcumin nanoformulations have demonstrated improved stability, enhanced cellular uptake, and superior anti-inflammatory activity compared with free curcumin in preclinical settings.

Within this framework, combining a standardized *M. malabathricum* leaf extract with nanocurcumin represents a mechanistically grounded strategy to pursue pharmacodynamic synergy and practical dose reduction. Polyphenol-rich botanical extracts and curcumin modulate overlapping yet non-identical nodes within the cytokine-COX-2/PGE_2-iNOS/NO-ROS network, potentially disrupting feed-forward loops linking oxidative stress, mediator amplification, nociceptive sensitization, and thermoregulatory signaling. If genuine synergy exists, the combination should permit lower doses of one or both components to achieve defined effect levels. Importantly, synergy should not be inferred from statistical significance alone; it requires quantitative interaction analysis across dose-effect relationships. The Chou-Talalay framework addresses this through the combination index (CI), which classifies synergism, additivity, or antagonism, and the dose-reduction index (DRI), which quantifies dose-sparing at specified fractional effects.

Despite a strong mechanistic premise, few studies integrate rigorous botanical authentication and chemical fingerprinting, comprehensive nanocurcumin physicochemical characterization, CI/DRI-based interaction analysis, and multi-model *in vivo* validation across pain, inflammation, and fever within a single coherent experimental pipeline. Therefore, the present study aimed to quality-control a standardized *M. malabathricum* leaf extract and a nanocurcumin formulation, establish single-agent dose-response relationships, quantify extract-nanocurcumin interactions using Chou-Talalay analysis, and validate efficacy in mice using complementary models of nociception, inflammation, and pyrexia supported by mechanistic biomarkers and safety assessment. We hypothesized that the combination would demonstrate CI < 1 with DRI > 1 at relevant effect levels and translate into concurrent analgesic, anti-inflammatory,

and antipyretic benefits accompanied by mediator changes consistent with multi-target network modulation and short-term tolerability under the study conditions.

2. MATERIALS AND METHODS

2.1. Study design, ethics, randomization and blinding

This study followed a predefined, stepwise pipeline: (i) quality control (QC) of a standardized *Melastoma malabathricum* leaf extract (ME) and a PLGA-based nanocurcumin formulation (NC); (ii) single-agent dose–response modeling and Chou-Talalay interaction analysis in a core *in vitro* anti-inflammatory assay; (iii) *in vivo* validation across pain, inflammation, and fever models in mice using prespecified derived endpoints; and (iv) mechanistic biomarker and safety assessments. The study is reported in accordance with ARRIVE 2.0.[9]

All animal procedures were approved by the Institutional Animal Ethics Committee (Approval No. 206DH/DHNN). Humane endpoints and exclusion criteria were prespecified. Animals were allocated to groups using computer-generated block randomization (block size = 5, corresponding to the five treatment groups), and outcome assessment (behavioral scoring, plethysmometry, temperature recording) was performed by an investigator blinded to treatment allocation.[10]

For each *in vivo* efficacy model, animals were assigned to five groups (vehicle, positive control, ME, NC, and ME+NC) with n = 6/group (30 animals/model). Across four independent efficacy models (hot-plate, formalin, carrageenan paw edema, and Brewer's yeast-induced pyrexia), this corresponded to 120 animals in total. To avoid carryover, independent cohorts were used for each *in vivo* model (i.e., animals were not reused across different efficacy models). A separate 14-day tolerability cohort (vehicle, ME, NC, and ME+NC; n = 6/group; total n = 24), which received test articles without any disease-model induction, was used exclusively for safety outcomes (body weight, serum biochemistry, and organ histopathology; Figure 6) to avoid confounding from the acute pharmacological challenges applied in the efficacy models.

2.2. Preparation and quality control of *M. malabathricum* leaf extract (ME) and nanocurcumin (NC)

2.2.1. Plant material authentication and extraction of ME (hydroethanolic extract)

Fresh leaves of *M. malabathricum* were collected in Ben Luc Commune, Long An Province, Vietnam (July 2025). Botanical identification was performed by a taxonomist, and a voucher specimen was deposited (ME150725VST). Leaves were washed, air-dried to constant weight, milled, and stored protected from light and moisture.

Powdered leaves were extracted with 70% ethanol (v/v) at a 1:10 (w/v) plant-to-solvent ratio using ultrasound-assisted extraction (30 min, 40 °C), repeated three times. Combined filtrates were concentrated under reduced pressure (≤ 45 °C) and freeze-dried to obtain ME powder. Extraction yield was defined as:

$$\text{Yield (\%)} = \frac{\text{Mass of freeze-dried extract}}{\text{Mass of dried plant powder}} \times 100$$

Observed yields across three independent batches were 12%.

2.2.2. ME standardization (TPC/TFC) and chromatographic fingerprinting

To ensure batch-to-batch consistency, ME was standardized using total phenolic content (TPC), total flavonoid content (TFC) and chromatographic fingerprint similarity.

TPC (Folin-Ciocalteu)

ME (1 mg/mL) was reacted with diluted Folin reagent, followed by 7.5% Na_2CO_3; absorbance was measured at 765 nm. Gallic acid calibration was used, and results were expressed as mg GAE/g extract.[11]

TFC ($AlCl_3$ method)

ME (1 mg/mL) was reacted with 2% $AlCl_3$; absorbance was measured at 415 nm. Quercetin calibration was used, and results were expressed as mg QE/g extract[12].

HPLC/UPLC fingerprinting

ME (1 mg/mL) in HPLC-grade methanol was sonicated and filtered (0.22 µm PTFE). Analyses were performed on a C18 column using water + 0.1% formic acid (A) and acetonitrile + 0.1% formic acid (B) with a linear gradient; DAD detection at 254/280/330 nm.[13]

Fingerprint similarity was assessed by overlaying chromatograms and by RSD% of retention times and peak areas for ≥ 5 major peaks (acceptance: RSD ≤ 5% for retention time and ≤ 10% for peak area).

Prespecified QC acceptance criteria.

Based on the observed batch clustering in Results (3.1), batches were accepted for biological testing if they met: Yield ≥ 12%; TPC ≥ 180 mg GAE/g; TFC ≥ 85 mg QE/g; marker compound content 42 ± 10 mg/g; and fingerprint similarity index ≥ 0.90.

2.2.3. Fabrication and characterization of nanocurcumin (NC)

NC was prepared by nanoprecipitation

Curcumin and PLGA (50:50) were dissolved in acetone (curcumin: PLGA = 1:10, w/w; polymer 5 mg/mL) and added dropwise (0.5 mL/min) into 1% (w/v) PVA under stirring (800 rpm) at room temperature (organic: aqueous = 1:5, v/v). The dispersion was stirred for 4 h to evaporate solvent, then centrifuged (15,000×g, 30 min, 4 °C), washed twice, resuspended in water and stored at 4 °C protected from light.

Particle size / PDI / zeta potential

Hydrodynamic diameter and PDI were measured by DLS; zeta potential was measured by electrophoretic light scattering (triplicate; ≥ 3 independent batches).

Morphology

For TEM imaging, NC suspensions were deposited onto conductive carbon tape, air-dried under dust-free conditions, sputter-coated with a thin conductive layer (Au/Pd), and imaged under high-vacuum conditions at an appropriate accelerating voltage with scale bars recorded. TEM images were used to assess particle morphology and aggregation status (Figure 2D).

Encapsulation efficiency (EE) and drug loading (DL). Curcumin was quantified after nanoparticle disruption (HPLC or UV-Vis at 425 nm against a curcumin standard), and calculated as:

$$\text{EE (\%)} = \frac{\text{Amount of curcumin encapsulated}}{\text{Total curcumin added}} \times 100$$

$$\text{DL (\%)} = \frac{\text{Amount of curcumin encapsulated}}{\text{Total weight of nanoparticles}} \times 100$$

In Results (3.1), EE clustered at 80-86% and DL around 9% across batches.

***In vitro* release**

Dialysis (MWCO 12-14 kDa) in PBS pH 7.4 + 0.5% Tween 80 at 37 °C, 100 rpm, under sink conditions; sampling with replacement; curcumin quantified by HPLC/UV-Vis. Sustained release was confirmed with ~90% cumulative release by 48 h for NC (free curcumin: near-complete release within 8-10 h).

QC governance

Prespecified NC acceptance criteria were: DLS size ≤ 200 nm, PDI ≤ 0.30, |zeta potential| ≥ 25 mV, EE ≥ 70%, DL ≥ 5%, burst release ≤ 30% (0-2 h), and stability drift ≤ 10% over storage (28-90 days), consistent with Table 1 structure and the observed QC ranges in Results (3.1).

2.3. Core *in vitro* anti-inflammatory assay and Chou-Talalay interaction analysis

2.3.1. Cell culture, LPS stimulation and readouts

RAW 264.7 murine macrophages were cultured in DMEM (high glucose) supplemented with 10% heat-inactivated FBS and 1% penicillin–streptomycin at 37 °C with 5% CO_2 Cells were seeded at 1.0×10^5 cells/well (96-well plates) and allowed to adhere overnight.[14]

Cells were pretreated with ME, NC, or fixed-ratio combinations for 2 h, then stimulated with LPS (E. coli O111:B4, 1 μg/mL) for 24 h. Nitrite accumulation was quantified by the Griess assay at 540 nm using a sodium nitrite standard curve. Cytokines (TNF-α, IL-6, IL-10, where applicable) were measured by ELISA according to the manufacturer's instructions. Cell viability was monitored using MTT; only concentrations maintaining ≥ 80% viability were included in synergy modeling. All experiments were performed in triplicate wells and repeated in ≥ 3 independent experiments.[14]

2.3.2. Fraction affected (Fa) and median-effect modeling

Fa was computed from the primary inhibitory endpoint (e.g., nitrite or cytokine) as:

$$Fa = \frac{R_{LPS} - R_{treatment}}{R_{LPS}}$$

; Fu = 1 - Fa, where R_{LPS} is the mean response in the LPS-only group, and $R_{treated}$ is the response under treatment.

Single-agent dose-response data (≥ 5-7 log-spaced concentrations) were fitted using the Chou-Talalay median-effect equation: $Fa/Fu = (D/Dm)^m$, (log form: $\log(Fa/Fu) = m\cdot\log(D) - m\cdot\log(D_m)$), where D is dose, Dm is the median-effect dose, and m is the slope; goodness-of-fit was assessed by r.[15]

2.3.3. Fixed-ratio combination design and CI/DRI computation

ME and NC were combined at a constant ratio derived from their single-agent D_m values (D_{mME}: D_{mNC}). Using the fitted Dm values reported in Table 2A (6.3 μg/mL vs 2.1 μg/mL), the working fixed ratio was approximately 3:1 (ME: NC, by concentration) for the *in vitro* CI/DRI analyses. Fixed-ratio combinations were tested over 1/8×, 1/4×, 1/2×, 1×, and 2× of the reference combination dose (defined as Fa ≈ 0.50) to generate Fa

values of 0.20-0.90. CI and DRI were computed using CompuSyn (v1.0) or validated equivalent software; interactions were classified as synergistic (CI < 1), additive (CI ≈ 1), or antagonistic (CI > 1).

2.4. *In vivo* efficacy in mice

2.4.1. Animals, housing, randomization, grouping and dosing

Male Swiss albino mice (6-8 weeks, 28-30 g) were obtained from the Pasteur Institute (Ho Chi Minh City) and housed under controlled conditions (22-25 °C; 50-70% humidity; 12 h light/dark cycle) with ad libitum access to standard chow and water. Animals were acclimatized for ≥ 7 days before experiments.

For each *in vivo* model, mice were randomized into five groups (n = 6/group): (i) vehicle control, (ii) model-matched positive control, (iii) ME, (iv) NC, and (v) ME+NC. Treatments were administered by oral gavage (10 mL/kg) in a consistent vehicle (0.5% CMC) unless otherwise specified.

Test articles

ME: 200 mg/kg, p.o. (expressed as dried extract mass); NC: 50 mg/kg, p.o. (expressed as curcumin-equivalent dose); ME+NC: 200 mg/kg ME + 50 mg/kg curcumin-equivalent NC, p.o., using a constant-ratio design aligned to the *in vitro* Dm-derived ratio (Section 2.3.3). The dose of ME (200 mg/kg) was selected within the effective range (100-400 mg/kg) reported for hydroethanolic *M. malabathricum* leaf extracts in murine antinociceptive and anti-inflammatory models (Ref. 5, 16), using a mid-range level to enable detection of combination-related enhancement without ceiling effects. The NC dose (50 mg/kg curcumin-equivalent) was based on PLGA-nanocurcumin studies demonstrating anti-inflammatory efficacy in rodents at comparable doses (Ref. 22) and was chosen as a sub-maximal dose to permit dose-sparing detection. The *in vivo* ratio (ME: NC ≈ 4:1 by mass) was aligned to the *in vitro* Dm-derived ratio (3:1 by concentration; Section 2.3.3) to maintain translational coherence.

Model-matched positive controls

Analgesia (hot-plate and formalin): tramadol hydrochloride 20 mg/kg, s.c., administered 30 min before testing.[16] Inflammation (carrageenan paw edema): meloxicam 3 mg/kg, p.o., administered 60 min before carrageenan injection.[17] Fever (Brewer's yeast pyrexia): paracetamol 150 mg/kg, p.o., administered at 0 h after fever confirmation; rectal temperature monitored for 0-6 h post-dose.[18]

2.4.2. Hot-plate test

The hot plate was maintained at 55 ± 1 °C. Baseline latency (L_0) was recorded immediately before dosing. Post-dose response latency (paw licking or jumping) was measured at 0.5, 1, 2, 4, and 6 h (cut-off: 30 s). Tramadol (20 mg/kg, s.c.) was administered 30 min before the first post-dose measurement as the positive control. Antinociception was expressed as the maximum possible effect:

$$\% \text{ MPE} = \frac{L_t - L_0}{L_{cutoff} - L_0} \times 100$$

Where Lt is the latency at time t, and L_{cutoff} is the cut-off latency.[16]

2.4.3. Formalin test

Formalin (20 µL, 2.5% v/v) was injected subplantarly. Treatments were administered 30-60 min before formalin injection; tramadol (20 mg/kg, s.c.) was administered 30 min prior as the positive control. Nociceptive behavior (licking/biting time) was recorded during Phase I (0-5 min) and Phase II (15-30 min). Analgesic activity was expressed as percent inhibition versus vehicle:

$$\% \text{ Inhibition} = \frac{T_c - T_t}{T_c} \times 100$$

Where T_c and T_t denote licking time in control and treated groups, respectively.[16]

2.4.4. Carrageenan-induced paw edema

Carrageenan (1% w/v, 50 µL) was injected subplantarly to induce acute inflammation. Meloxicam (3 mg/kg, p.o.) was administered 60 min before carrageenan injection as the positive control. Paw volume was measured at baseline (V_o) and at 1-6 h post-injection (V_t) using plethysmometry. Edema was calculated as

$$\Delta V_t = V_t - V_0.$$

Percent inhibition was calculated as:

$$\% \text{ Inhibition} = \frac{\Delta V_C - \Delta V_t}{\Delta V_c} \times 100$$

Where ΔV_c is the mean edema in the vehicle group at the corresponding time point.[17]

2.4.5. Brewer's yeast-induced pyrexia

Mice were fasted overnight with free access to water. Baseline rectal temperature was recorded, and

pyrexia was induced by Brewer's yeast (20% w/v in saline, 10 mL/kg, s.c.). After 18 h, only animals exhibiting a ≥ 0.5 °C increase were included. Paracetamol (150 mg/kg, p.o.) was administered at 0 h (post-yeast, pre-treatment baseline) as the positive control. Rectal temperature was recorded at 0, 1, 2, 3, 4 and 6 h post-treatment.

Antipyretic response was expressed as ΔT (°C) relative to the post-yeast, pre-treatment value.[18]

2.4.6. Prespecified derived endpoints

To avoid redundancy with time-course plots, primary efficacy was summarized using prespecified derived endpoints: Hot-plate: $AUC_{\%MPE}$ over 0-6h (units: %·h), with E_{max} and T_{max} reported as supportive metrics. Formalin: phase-specific % inhibition for Phase I (0-5 min) and Phase II (15-30 min). Carrageenan edema: $AUC_{\%inhibition}$ (0-6 h) (units: %·h) and % inhibition at 3-4 h (prespecified peak window). Pyrexia: $AUC_{\Delta T}$ (0-6 h) (units: °C·h) and maximum ΔT reduction (°C). AUC was calculated using the trapezoidal rule:

$$AUC = \sum_{i=1}^{n-1} \frac{(y_i + y_{i+1})}{2} (t_{i+1} - t_i)$$

2.5. Mechanistic biomarkers

2.5.1. Sample collection and processing

Sampling timepoints were aligned to model kinetics: carrageenan (3-4 h post-injection, or at the end of the time-course if AUC was primary) and yeast pyrexia (typically 2-4 h post-treatment). Animals were anesthetized (ketamine/xylazine 80/10 mg/kg i.p. or isoflurane). Serum was collected and stored at -80 °C. Tissue (paw and/or organs) was snap-frozen and homogenized (10% w/v) in lysis buffer with protease inhibitors; protein was normalized by BCA/Bradford.

2.5.2. Cytokines, PGE_2 and COX-2/iNOS

Serum/tissue TNF-α, IL-1β, and IL-6 were quantified by sandwich ELISA; PGE_2 by ELISA where applicable. Results were expressed as pg/mL (serum) or pg/mg total protein (tissue). COX-2 and iNOS were measured by qPCR (2^−ΔΔCt with GAPDH/β-actin normalization) and/or Western blot (30-40 µg protein; PVDF; normalized to β-actin/GAPDH).[14]

2.5.3. Oxidative stress markers

MDA (TBARS), SOD, CAT, and GSH were measured using validated kits or standardized spectrophotometric assays and normalized to protein.[19]

2.6. Safety assessment

Animals were monitored daily for clinical signs; body weight was recorded longitudinally. Serum ALT, AST and urea/creatinine were measured using validated chemistry assays. Liver and kidney histology (H&E) was performed with blinded evaluation. Group-level safety summaries were presented in Figure 6, with full numeric data provided in Supplementary Table S1.[20]

For histopathological assessment, liver and kidney tissues were harvested at day 14 from a subset of animals (n = 6 per group), fixed in 10% neutral-buffered formalin, processed routinely, embedded in paraffin, sectioned at 4-5 µm, and stained with hematoxylin and eosin. Sections were examined under light microscopy at 200× magnification. Histological evaluation was performed in a blinded manner by an experienced pathologist, with qualitative assessment of tissue architecture, inflammatory cell infiltration, hepatocellular integrity, glomerular and tubular morphology, and evidence of necrosis or degeneration. Representative images are shown in Figure 6D.

2.7. Statistics and data handling

Analyses were conducted in GraphPad Prism (v9.5.1) and, where applicable, R (v4.3.1). Normality and variance assumptions were checked (Shapiro-Wilk; Levene). Time-course outcomes were analyzed by two-way repeated-measures ANOVA; mixed-effects models (REML) were used for missing values. Multiple comparisons were controlled using Tukey's HSD or Holm's correction as prespecified. Effect sizes (η^2/partial η^2; Cohen's d, where applicable) were reported alongside p-values.

3. RESULTS

3.1. Input authentication and quality control of ME and NC

Prespecified quality-control (QC) elements for botanical authentication, extract standardization, and nanocurcumin performance are summarized in Table 1. Three independent batches of *M. malabathricum* leaf extract (ME) demonstrated consistent extraction yields (12-13%) and closely aligned chemical indices, including total phenolic content (TPC, 180-190 mg GAE/g), total flavonoid content (TFC, 85-95 mg QE/g), and marker content (41-43 mg/g), together with highly superimposable HPLC fingerprints (Figure 1).

For nanocurcumin (NC), dynamic light scattering (DLS) showed a unimodal size distribution centered at 150-170 nm and a stable negative zeta potential (-30 to -33 mV). Encapsulation efficiency was

Table 1. Prespecified quality control (QC) specifications for *Melastoma malabathricum* leaf extract (ME) and nanocurcumin (NC).

Category	Parameter	Method / Reference	Acceptance criteria
Botanical authentication	Voucher specimen	Deposited at an accredited herbarium; taxonomist identification	Voucher number recorded; species confirmed
	Plant part	Macroscopic & microscopic examination	Leaves (as specified)
	Moisture content	Loss on drying (AOAC)	≤ 12%
	Foreign matter	Gravimetric	≤ 2%
Extraction (ME)	Extraction solvent	70% ethanol (v/v)	Fixed composition
	Extraction method	Ultrasound-assisted extraction	30 min at 40 °C
	Drug-to-solvent ratio	Gravimetric	1:10 (w/v)
	Extraction yield	Gravimetric	≥ 12% (batch mean ± SD)
Chemical standardization (ME)	Total phenolic content (TPC)	Folin-Ciocalteu assay	≥ 180 mg GAE/g extract
	Total flavonoid content (TFC)	$AlCl_3$ colorimetric assay	≥ 85 mg QE/g extract
	Marker compound content	HPLC/UHPLC (validated)	42 ± 10 mg/g extract
	HPLC fingerprint similarity	Chromatographic fingerprinting	≥ 0.90
Chromatographic fingerprint (ME)	Column	C18 reversed-phase	Fixed specification
	Detection wavelength(s)	DAD	254 / 280 / 330 nm
	Major peak RRT	Relative retention time	RSD ≤ 5%
	Peak area reproducibility	Fingerprint similarity	RSD ≤ 10%
Nanoparticle formulation (NC)	Fabrication method	Nanoprecipitation (PLGA-curcumin)	Fixed protocol
	Curcumin: polymer ratio	Gravimetric	1:10 (w/w)
Physicochemical properties (NC)	Particle size (DLS)	Dynamic light scattering	≤ 200 nm
	Polydispersity index (PDI)	DLS	≤ 0.30
	Zeta potential	Electrophoretic light scattering	|zeta| ≥ 25 mV
	Particle size (TEM)	Transmission electron microscopy	Within ±20% of DLS
Encapsulation performance (NC)	Encapsulation efficiency (EE)	HPLC/UV-Vis	≥ 70%
	Drug loading (DL)	HPLC/UV-Vis	≥ 5%
Morphology (NC)	Shape and surface	TEM	Spherical, non-aggregated
In vitro release (NC)	Release medium	PBS pH 7.4 + 0.5% Tween 80	Sink conditions
	Release profile	Dialysis method	Sustained release; ≤ 30% burst (0-2 h)
	Release kinetics	Higuchi / Korsmeyer-Peppas	R^2 ≥ 0.95
Stability (NC)	Size & PDI drift	DLS after storage (28-90 days)	≤ 10% change
	Curcumin content	HPLC after storage	≥ 90% of initial content
Safety	Microbial limits	USP <61>/<62>	Complies with limits
	Endotoxin level	LAL assay	≤ acceptable limit
Batch reproducibility	Inter-batch variation	≥ 3 independent batches	Meets all QC criteria

The table summarizes QC categories, analytical methods/references, and acceptance criteria covering botanical authentication, extract standardization (yield, TPC/TFC, marker content), chromatographic fingerprint similarity, NC formulation parameters (DLS size/PDI, zeta potential, EE/DL, morphology), *in vitro* release and kinetic fitting, stability checks, and basic safety-related limits (microbial/endotoxin), with batch reproducibility assessed across ≥3 independent batches.

80-86% with drug loading around 9%, and microscopy indicated predominantly spherical particles with minimal aggregation (Figure 2). NC exhibited sustained curcumin release, reaching 90% at 48 h, whereas free curcumin approached near-complete release within 8-10 h. Collectively, these results confirm sufficient material consistency to support downstream interaction modeling and *in vivo* validation.

3.2. Single-agent dose-response and median-effect modeling in LPS-stimulated RAW 264.7 cells

Both ME and NC produced dose-dependent increases in fractional effect (Fa) in LPS-stimulated RAW 264.7 macrophages. Median-effect plots were approximately linear, supporting reliable parameter estimation (Figure 3A-B).

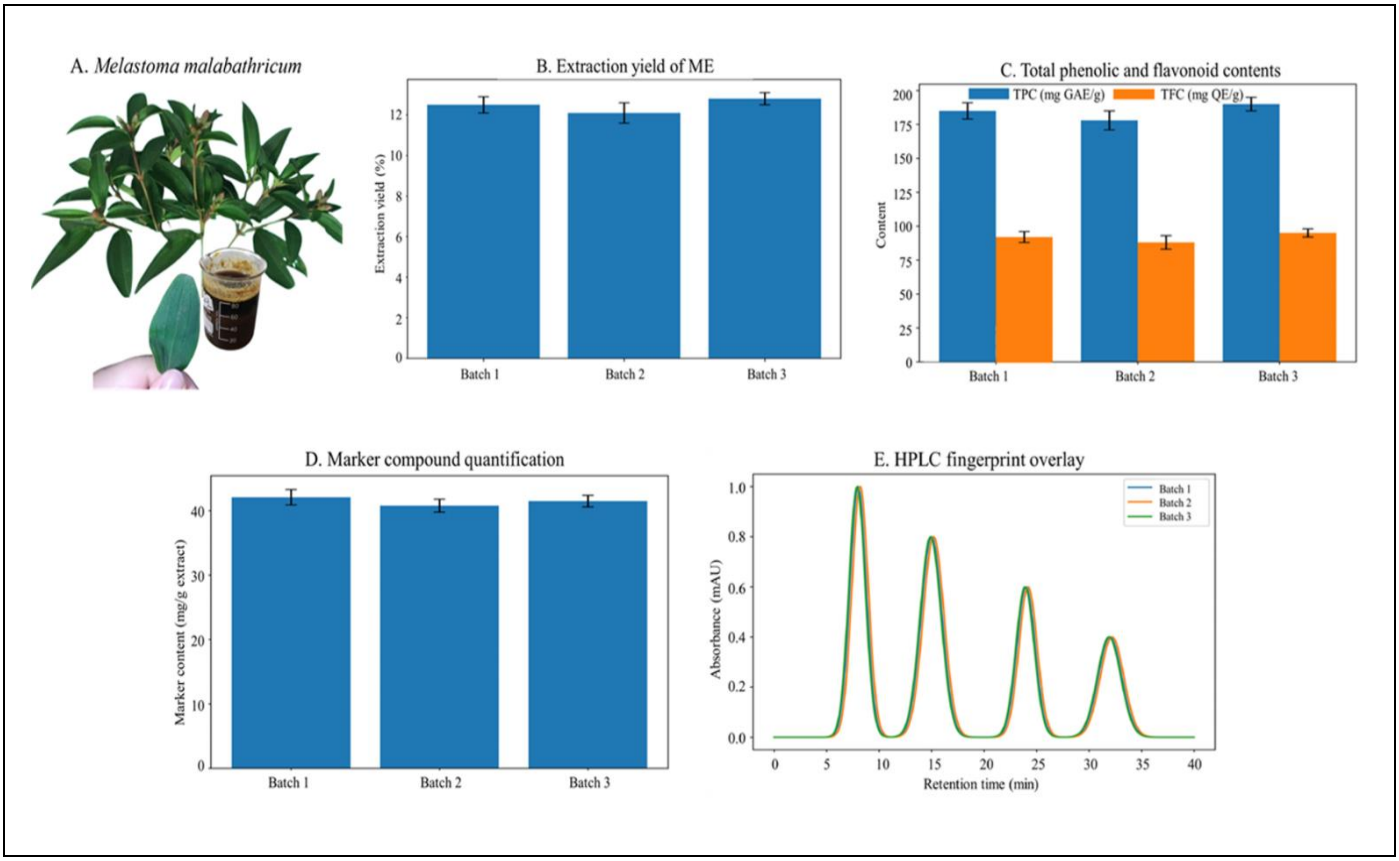

Figure 1. Batch-to-batch consistency and chemical standardization of a 70% ethanolic *Melastoma malabathricum* leaf extract (ME). (A) Representative plant material and the corresponding dried extract used for biological testing. (B) Extraction yield (%) across three independent batches. (C) Total phenolic content (TPC; mg GAE/g extract) and total flavonoid content (TFC; mg QE/g extract) were determined using Folin–Ciocalteu and $AlCl_3$ colorimetric assays, respectively. (D) Marker compound content (mg/g extract) quantified by external-standard calibration. (E) HPLC/UPLC-DAD fingerprint overlays demonstrating chromatographic similarity among ME batches (C18 column; water/acetonitrile with 0.1% formic acid gradient; DAD at 254/280/330 nm). Bar data are presented as mean ± SD from replicate measurements; fingerprint similarity was assessed by chromatogram overlay and RSD of retention time and peak area for ≥ 5 major peaks.

Median-effect parameters (Table 2A), where Dm corresponds to the IC50 (the concentration producing 50% of maximum inhibition), indicated good model fit for both agents: ME (m = 1.21 ± 0.08; Dm = 6.3 ± 0.5 µg/mL; r = 0.96) and NC (m = 1.38 ± 0.10; Dm = 2.1 ± 0.2 µg/mL; r = 0.97). These fitted parameters were used to define the fixed-ratio combination design and subsequent CI/DRI calculations.

3.3. Chou-Talalay interaction analysis demonstrates synergism and dose-sparing

Across key effect levels, the fixed-ratio ME+NC combination demonstrated synergistic interaction with practical dose-sparing for both components (Table 2B; Figure 3C–D). At Fa = 0.50, CI was 0.62 with DRI values of 2.6 (ME) and 3.0 (NC). At Fa = 0.75, CI was 0.79 with DRI values of 2.2 (ME) and 2.7 (NC). At Fa = 0.90, CI decreased to 0.58 with DRI values of 2.6 (ME) and 3.1 (NC). Together, these findings indicate consistent synergism across clinically relevant effect levels and confirm a meaningful dose-sparing profile.

3.4. *In vivo* analgesic efficacy in mice

Tramadol served as the model-matched positive control for central analgesia and produced the expected antinociceptive response, confirming assay sensitivity. Among the test articles, ME+NC showed the strongest antinociceptive profile in the hot-plate test (Figure 4A). As summarized in Table 3A, ME+NC achieved the highest overall analgesic effect (AUC%MPE = 98.4 ± 8.9) and peak effect (Emax = 65.3 ± 6.1), exceeding NC (AUC%MPE = 62.8 ± 7.4; Emax = 45.1 ± 5.0) and ME (AUC%MPE = 48.2 ± 6.1; Emax = 32.5 ± 4.2). Tramadol also produced robust antinociception, with an AUC%MPE of 85.0 ± 7.5 and an Emax of 58.0 ± 5.0 %MPE at a Tmax of 45 ± 8 min, corresponding to a very large effect size relative to vehicle (Cohen's *d* = 2.00).

3.4.1. Formalin test

Tramadol served as the model-matched positive control and produced marked antinociception in both phases of the formalin test (Phase I: 40.0 ± 4.0%

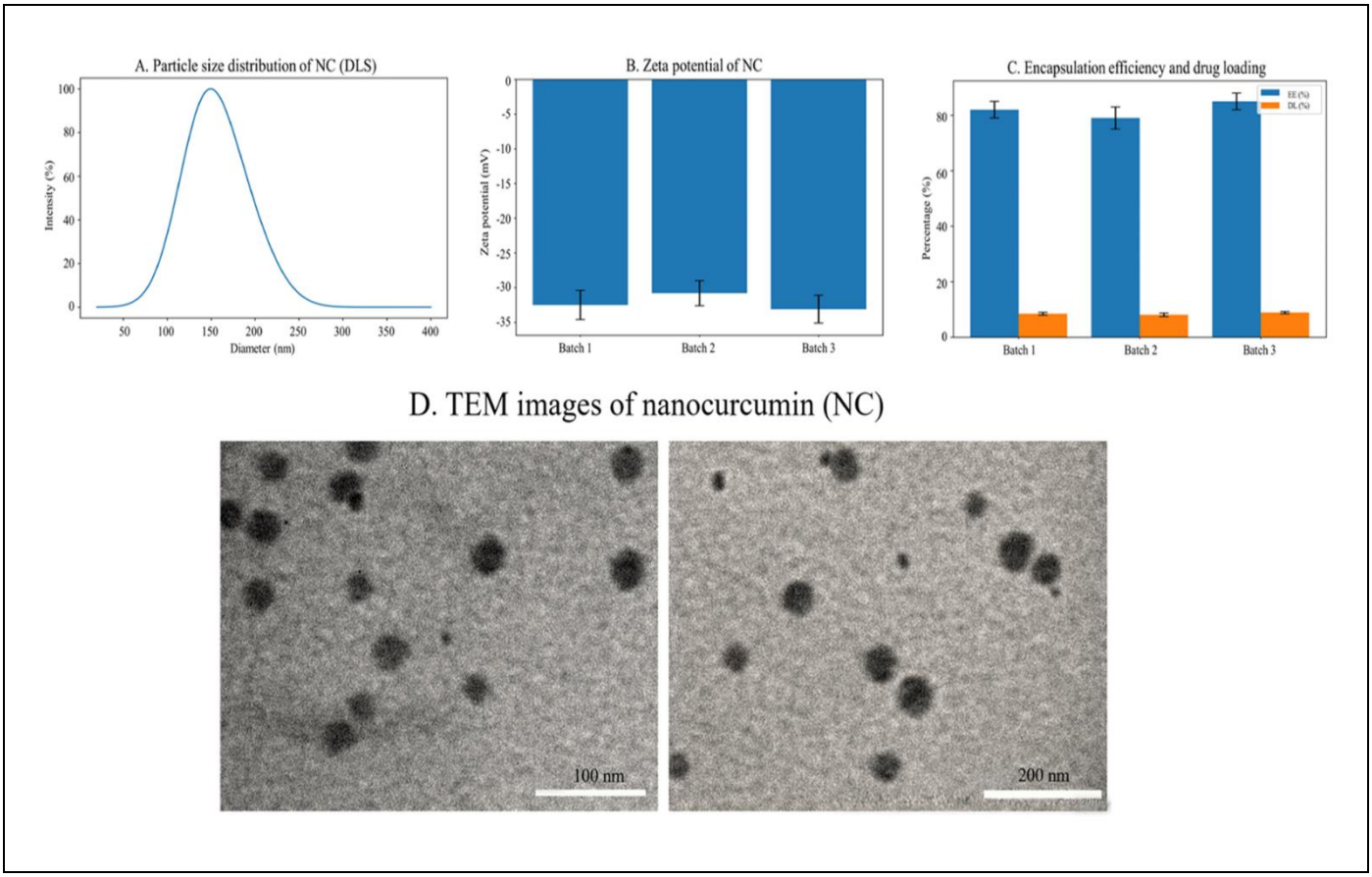

Figure 2. Physicochemical characterization and encapsulation performance of PLGA-based nanocurcumin (NC). (A) Representative particle size distribution of NC measured by dynamic light scattering (DLS; hydrodynamic diameter). (B) Zeta potential (mV) across three independent batches measured by electrophoretic light scattering. (C) Encapsulation efficiency (EE, %) and drug loading (DL, %) across batches were quantified against a curcumin standard. (D) Representative TEM micrographs showing predominantly spherical NC nanoparticles; scale bars are indicated on images. Data are presented as mean ± SD of replicate measurements; batch-to-batch measurements were obtained from ≥ 3 independent NC batches.

inhibition; Phase II: 52.0 ± 5.0%; Cohen's d = 1.90), confirming model responsiveness (Figure 4B; Table 3A). In the inflammatory Phase II (15-30 min), ME+NC produced the greatest inhibition among test articles (68.9 ± 5.3%; d = 2.20), exceeding NC (42.6 ± 4.1%; d = 1.45) (Table 3A). ME showed measurable antinociception in Phase I (0-5 min) with 28.4 ± 3.2% inhibition (d = 1.10) (Table 3A). Phase-specific outcomes are summarized in Table 3A.

3.5. *In vivo* anti-inflammatory and antipyretic efficacy

3.5.1. Carrageenan-induced paw edema

Meloxicam served as the model-matched positive control and reduced paw edema as expected, validating the carrageenan model (Figure 4C; Table 3B). ME+NC reduced paw edema most consistently across the time course (Figure 4C). Derived endpoints (Table 3B) showed the greatest overall activity for ME+NC (AUC% inhibition (0–6 h) = 45.2 ± 4.6 %·h) and the highest inhibition at 3–4 h (68.4 ± 6.1%), exceeding NC (AUC% inhibition (0–6 h) = 28.8 ± 3.8 %·h; 45.6 ± 5.2%) and ME (AUC% inhibition (0-6 h) = 22.5 ± 3.1 %·h; 34.2 ± 4.5%).

Positive control (Table 3B). Meloxicam produced a robust anti-inflammatory effect (AUC% inhibition (0–6 h) = 36.0 ± 4.0 %·h; 60.0 ± 5.0% inhibition at 3–4 h) with a very large effect size versus vehicle (Cohen's d = 2.00), confirming assay sensitivity.

3.5.2. Brewer's yeast-induced pyrexia

Paracetamol served as the reference antipyretic drug for the yeast pyrexia model. ME+NC produced the strongest antipyretic response (Figure 4D). Time-integrated fever reduction (Table 3C) was greatest for ME+NC ($AUC_{\Delta T}$ = 8.6 ± 0.9) compared with NC (5.1 ± 0.7) and ME (3.8 ± 0.6). Maximum temperature reduction (Max ΔT) also favored ME+NC (2.1 ± 0.4 °C) over NC (1.3 ± 0.3 °C) and ME (0.9 ± 0.2 °C).

Positive control (Table 3C). Paracetamol produced a pronounced antipyretic response ($AUC_{\Delta T}$, 0-6 h = 7.2 ± 0.8; maximum reduction = 1.9 ± 0.3 °C) with a very large effect size versus vehicle (Cohen's d = 2.00), confirming assay sensitivity.

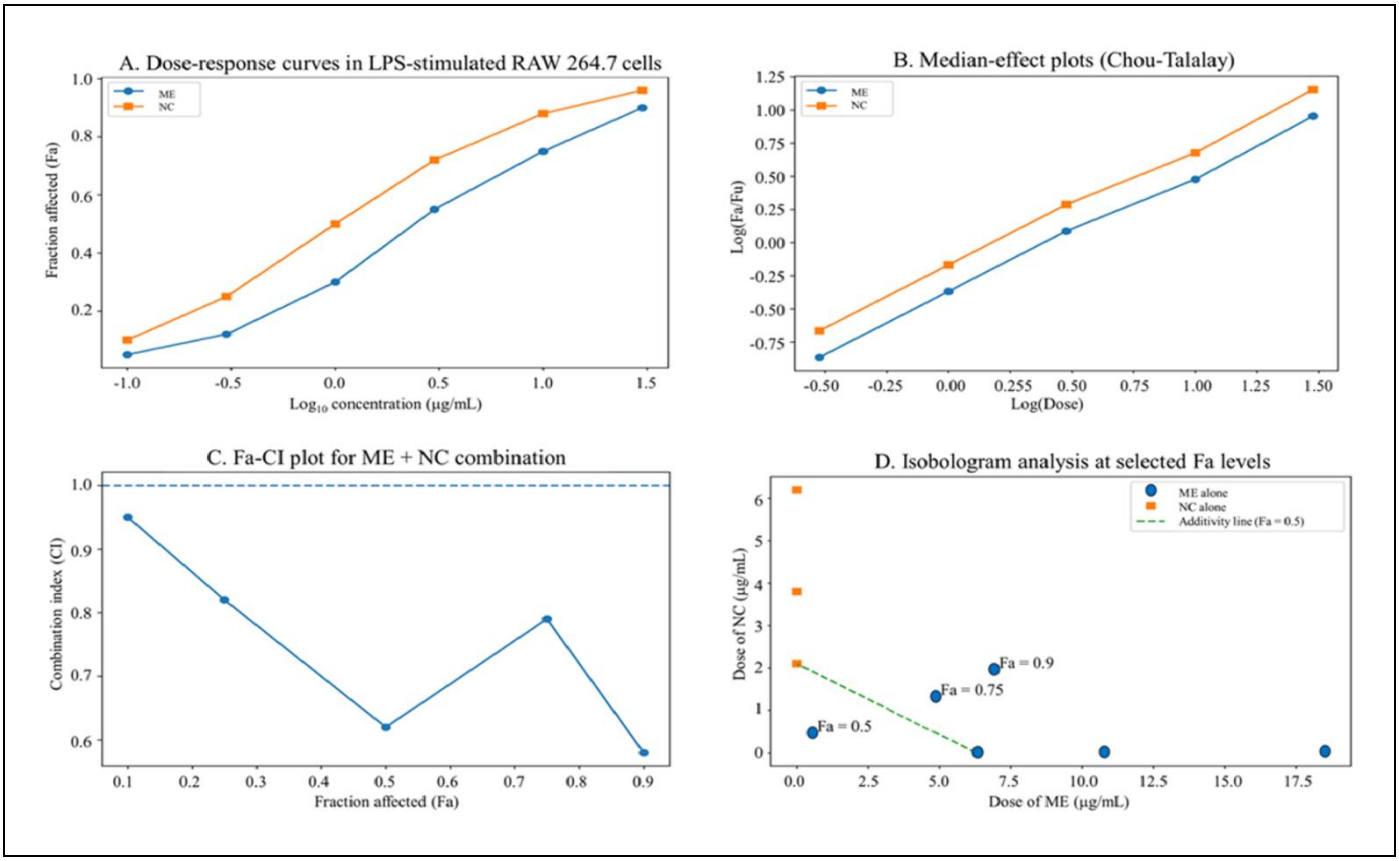

Figure 3. Single-agent dose–response modeling and Chou-Talalay interaction analysis for ME and nanocurcumin (NC) in LPS-stimulated RAW 264.7 macrophages. (A) Single-agent dose–response curves expressed as fraction affected (Fa) across log_{10} concentrations. RAW 264.7 cells were pretreated for 2 h, stimulated with LPS (E. coli O111:B4, 1 μg/mL) for 24 h, and nitrite accumulation was quantified using the Griess assay. (B) Median-effect plots [log(Fa/Fu) vs log(dose)] were used to estimate slope (m), median-effect dose (Dm), and correlation coefficient (r) for each agent (Table 2A). (C) Fa-CI plot for the fixed-ratio ME+NC combination; the horizontal line at CI = 1 indicates additivity (CI < 1, synergism; CI > 1, antagonism). (D) Isobologram at Fa 0.50, 0.75, and 0.90; points below the additivity line indicate synergism. Experiments were performed in triplicate wells and repeated in ≥ 3 independent experiments. Data are presented as mean ± SD.

3.6. Mechanistic biomarker changes associated with ME, NC and ME+NC treatment

Treatment with ME, NC, and especially their combination (ME+NC) significantly modulated inflammatory and oxidative stress biomarkers compared with the vehicle group (Figure 5, $p < 0.05$). As shown in Figure 5A, the levels of the pro-inflammatory cytokines TNF-α, IL-1β, and IL-6 were significantly reduced in all treated groups relative to vehicle, with the greatest decrease observed in the ME+NC group. Notably, the combination produced a more pronounced suppression of these cytokines than either ME or NC alone.

A similar trend was observed for inflammatory enzyme expression (Figure 5B). COX-2 and iNOS levels were significantly lower in the ME-, NC-, and meloxicam-treated groups than in the vehicle group, whereas the ME+NC group showed the strongest inhibitory effect overall ($p < 0.05$). These findings further support the enhanced anti-inflammatory activity of the combined treatment.

Table 2. Chou-Talalay median-effect parameters and combination metrics for *Melastoma malabathricum* hydroethanolic extract (ME) and nanocurcumin (NC) in LPS-stimulated RAW 264.7 cells.

Table 2A. Median-effect parameters of single agents, including slope (m), median-effect dose (Dm; ED50-equivalent), and correlation coefficient (r), derived from median-effect plots.

Agent	m (slope)	Dm (IC50/ED50-equivalent)	r (correlation)
ME	1.21 ± 0.08	6.3 ± 0.5 μg/mL	0.96
NC	1.38 ± 0.10	2.1 ± 0.2 μg/mL	0.97

Dm and m values were derived from median-effect plots (Figure 3B).

Table 2B. Combination index (CI) and dose reduction index (DRI)

Fa	Dose (ME) alone	Dose (NC) alone	Dose in combination (ME)	Dose in combination (NC)	CI	DRI (ME)	DRI (NC)	Interaction
0.50	6.3	2.1	2.4	0.7	0.62	2.6	3.0	Synergism
0.75	10.8	3.8	4.9	1.4	0.79	2.2	2.7	Synergism
0.90	18.5	6.2	7.1	2.0	0.58	2.6	3.1	Synergism

Values at selected fractional effects (Fa = 0.50, 0.75, 0.90), with "Dose (ME) alone" and "Dose (NC) alone" indicating the single-agent doses required to reach the same Fa, and "Dose in combination" indicating the component doses within the fixed-ratio combination. Doses are reported in µg/mL.

With respect to oxidative stress and antioxidant defense, ME+NC also demonstrated the most favorable biomarker profile (Figure 5C). MDA, a marker of lipid peroxidation, was significantly decreased, while endogenous antioxidant indices, including SOD, CAT, and GSH, were significantly increased compared with the vehicle group ($p < 0.05$). Although ME and NC alone also improved these parameters, the combined treatment produced the greatest overall reduction in oxidative stress together with the strongest enhancement of antioxidant defenses.

Taken together, these results indicate that the superior analgesic, anti-inflammatory, and antipyretic effects of ME+NC are associated with coordinated suppression of inflammatory mediators and reinforcement of antioxidant defense systems.

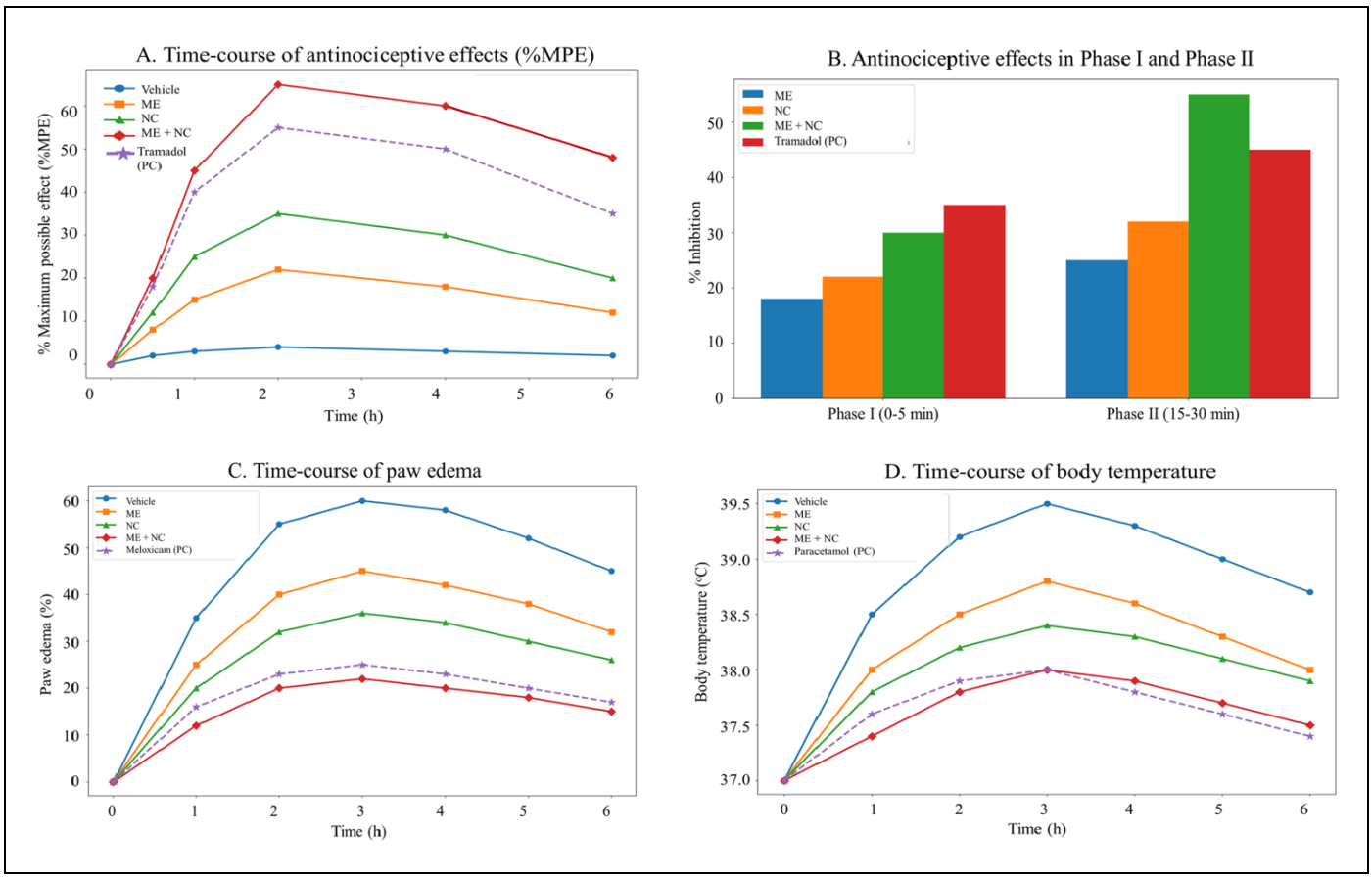

Figure 4. *In vivo* time-course efficacy of ME, nanocurcumin (NC), and ME+NC in Swiss albino mice across pain, inflammation, and fever models. (A) Hot-plate test: time-course of antinociceptive effects expressed as % maximum possible effect (%MPE). (B) Formalin test: antinociceptive effects expressed as percent inhibition of licking/biting time versus vehicle for Phase I (0–5 min) and Phase II (15–30 min). (C) Carrageenan-induced paw edema: time-course of paw edema expressed as paw edema (%) over time (see calculation methods). (D) Time-course of rectal temperature in the Brewer's yeast-induced pyrexia test (°C). Groups include vehicle, ME, NC, ME+NC, and the model-matched positive control (tramadol for A-B, meloxicam for C, and paracetamol for D; doses as described in Methods). Data are presented as mean ± SD (n = 6/group).

3.7. Safety outcomes and tolerability

During the 14-day observation period, body weight was maintained or gradually increased across all treatment groups, with no pattern suggestive of treatment-related wasting or overt systemic intolerance (Figure 6A). Animals receiving the ME+NC combination likewise showed progressive weight gain over time, consistent with good short-term tolerability during repeated administration.

Serum biochemical assessment supported good short-term tolerability of the tested treatments. Liver function biomarkers, including ALT and AST, remained close to vehicle values in the ME-, NC-, and ME+NC-treated groups, with no pattern suggestive of hepatotoxicity (Figure 6B). Likewise, kidney function biomarkers, urea and creatinine, were not adversely altered relative to the vehicle group, indicating no evidence of treatment-related renal biochemical disturbance under the study conditions (Figure 6C). Overall, no biologically meaningful adverse deviations were observed in these measured safety-related parameters.

Histopathological observations were consistent with the biochemical data. Representative H&E-stained sections of liver and kidney from the vehicle and ME+NC groups did not reveal obvious treatment-related qualitative abnormalities, including overt tissue injury, inflammatory infiltration, necrosis, or structural distortion in the examined fields (Figure 6D). The overall microscopic appearance of the ME+NC group was comparable to that of the vehicle group in the representative sections examined.

Taken together, these findings indicate that the combination of ME and NC was well tolerated during the 14-day study period and was not associated with overt toxicity in the measured biochemical and histopathological endpoints under the study conditions.

Table 3. *In vivo* derived efficacy endpoints and effect sizes across pain, inflammation, and fever models in Swiss albino mice.

Table 3A. Analgesia models: hot-plate AUC%MPE and Emax; formalin Phase I and Phase II inhibition (%).

Model	Treatment	$AUC_{\%MPE}$ (0-6h) / % Inhibition	Hot-plate: E_max (%MPE) / Formalin: % inhibition	T_{max} (min)	Effect size vs. vehicle (Cohen's d)
Hot-plate	Vehicle	—	—	—	—
	Tramadol	85.0 ± 7.5	58.0 ± 5.0	45 ± 8	2.00
	ME	48.2 ± 6.1	32.5 ± 4.2	60 ± 10	1.25
	NC	62.8 ± 7.4	45.1 ± 5.0	45 ± 8	1.62
	ME + NC	98.4 ± 8.9	65.3 ± 6.1	30 ± 6	2.45
Formalin	Vehicle	—	—	—	—
	Tramadol	—	Phase I: 40.0 ± 4.0; Phase II: 52.0 ± 5.0		
	ME	—	Phase I: 28.4 ± 3.2; Phase II: 35.6 ± 3.8		
	NC	—	Phase I: 18.9 ± 2.7; Phase II: 42.6 ± 4.1		
	ME + NC	—	Phase I: 46.3 ± 4.5; Phase II: 68.9 ± 5.3		

Data are presented as mean ± SD (n = 6/group). Hot-plate AUC%MPE (0-6 h) was calculated using the trapezoidal rule. Formalin antinociception is expressed as percent inhibition of licking/biting time versus vehicle: % inhibition = [(Tc − Tt)/Tc] × 100. For the formalin test, Cohen's d is reported for Phase II.

Table 3B. Inflammation model (carrageenan paw edema): AUC% inhibition (0–6 h) and % inhibition at 3–4 h.

Model	Treatment	$AUC_{\%\ inhibition}$ (0-6 h)	% inhibition at 3-4 h	Effect size vs. vehicle (Cohen's d)
Carrageenan paw edema	Vehicle	—	—	—
	Meloxicam	36.0 ± 4.0	60.0 ± 5.0	2.00
	ME	22.5 ± 3.1	34.2 ± 4.5	1.30
	NC	28.8 ± 3.8	45.6 ± 5.2	1.65
	ME + NC	45.2 ± 4.6	68.4 ± 6.1	2.50

Data are presented as mean ± SD (n = 6/group). AUC% inhibition (0–6 h) was calculated using the trapezoidal rule from the time-course of percent inhibition of paw edema versus vehicle across the 0–6 h observation period. Percent inhibition at 3–4 h was calculated versus vehicle. Effect sizes are reported as Cohen's d versus vehicle.

Table 3C. Fever model (Brewer's yeast pyrexia): AUCΔT (0-6 h) and maximum ΔT reduction (°C). Effect sizes are reported as Cohen's d versus vehicle.

Model	Treatment	AUC_ΔT (0-6 h)	Max ΔT reduction (°C)	Effect size vs. vehicle (Cohen's d)
Brewer's yeast pyrexia	Vehicle	—	—	—
	Paracetamol	7.2 ± 0.8	1.9 ± 0.3	2.00
	ME	3.8 ± 0.6	0.9 ± 0.2	1.15
	NC	5.1 ± 0.7	1.3 ± 0.3	1.48
	ME + NC	8.6 ± 0.9	2.1 ± 0.4	2.35

Data are presented as mean ± SD (n = 6/group). AUCΔT (0-6 h) was calculated using the trapezoidal rule from temperature reductions over time. Maximum ΔT reduction is the largest decrease from the post-yeast, pretreatment baseline; Cohen's d is versus vehicle.

4. DISCUSSION

This study integrates (i) quality control and batch consistency for a standardized botanical extract and a nanocurcumin formulation, (ii) quantitative interaction analysis using the Chou-Talalay dose–effect framework, and (iii) multi-model *in vivo* validation across pain, inflammation, and fever in mice.[21] The key finding is that ME+NC exhibits CI-defined synergism with meaningful dose-sparing (DRI) in the core inflammatory assay, and this interaction is mirrored by coherent *in vivo* efficacy, concordant biomarker modulation, and no overt safety signals within the observation window.

A major strength is the inclusion of pharmacologically appropriate positive controls in each *in vivo* model: tramadol for analgesia, meloxicam for carrageenan-induced inflammation, and paracetamol for pyrexia, which confirmed assay sensitivity and provided an internal benchmark for interpreting effect magnitude.[22] By anchoring interpretation to these reference responses, the study reduces the risk that apparent group separation reflects procedural variability rather than true pharmacodynamic activity.[23]

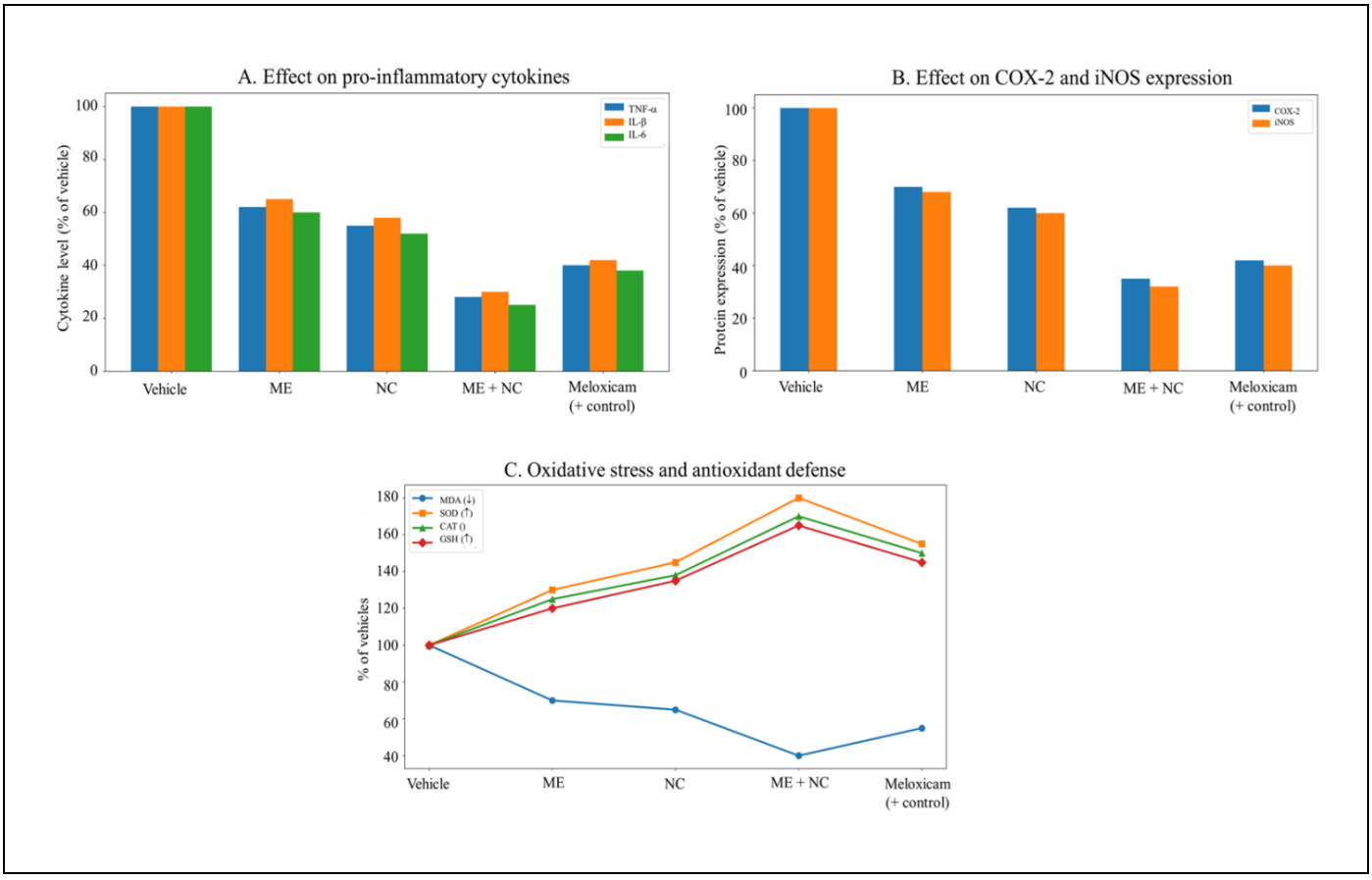

Figure 5. Effects of ME, nanocurcumin (NC), and ME+NC on inflammatory mediators and oxidative stress biomarkers. (A) Pro-inflammatory cytokines (TNF-α, IL-1β, IL-6). (B) COX-2 and iNOS expression. (C) Oxidative stress and antioxidant defense indices, including MDA, SOD, CAT, and GSH. Results are expressed as a percentage of the vehicle group (vehicle = 100%). Groups include vehicle, meloxicam, ME, NC, and ME+NC. Data are presented as mean ± SD (n = 6/group).

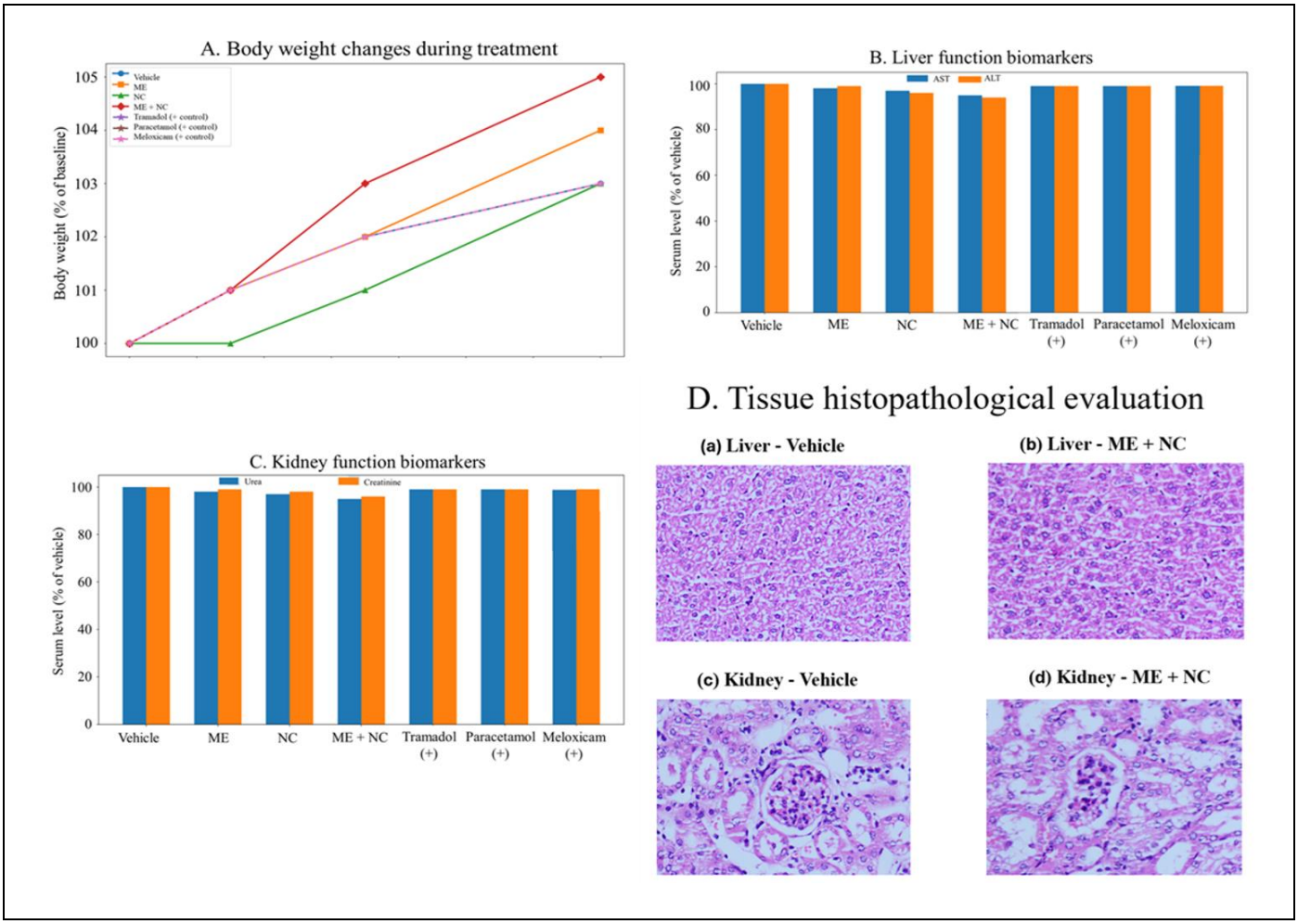

Figure 6. Safety and tolerability assessment of ME, nanocurcumin (NC), and ME+NC in Swiss albino mice. (A) Body weight during the 14-day observation period, expressed as a percentage of baseline (day 0 = 100%). (B) Serum liver biomarkers (ALT and AST) and (C) serum kidney biomarkers (urea and creatinine) expressed as a percentage of the vehicle group (vehicle = 100%); absolute values are provided in Supplementary Table S1. (D) Representative H&E-stained sections of liver and kidney from vehicle and ME+NC groups (200×; scale bars as indicated). No obvious treatment-related abnormalities were noted in the representative sections examined under the study conditions. Images are representative of n = 6 animals per group.

Credible interaction claims also depend on reproducible inputs. Batch-to-batch drift in botanical mixtures and nanoformulations can confound interpretation and may be misconstrued as "synergy" if not controlled.[24] Here, ME batches showed consistent yield and aligned chemical indices (TPC/TFC, marker content, and fingerprint similarity), while NC demonstrated stable physicochemical attributes (size, zeta potential, EE/DL) and sustained release relative to free curcumin. These QC measures align with current expectations for herbal standardization based on fingerprinting/chemometrics and for nanoformulation performance supported by size distribution, PDI, surface charge, entrapment efficiency, drug loading, stability, and release profiling.[25]

Beyond demonstrating that "the combination performs better," the study quantifies interaction within a dose-effect framework. Median-effect modeling supported a fixed-ratio combination design for CI and DRI computation, and CI/DRI reporting is widely used to classify synergism and practical dose-sparing in combination studies.[26] In the present work, CI remained < 1 across relevant effect levels, while DRI indicated 2-3-fold dose reductions for both components, translating synergy into an actionable dose-sparing interpretation rather than a purely statistical comparison.

The *in vivo* findings were consistent across complementary models and interpretable relative to positive-control benchmarks. ME+NC produced the strongest overall antinociceptive profile in the hot-plate assay (highest $AUC_{\%MPE}$ and E_{max} among test articles), and it showed the greatest Phase II effect in the formalin test, supporting improved control of inflammatory sensitization. In carrageenan-induced edema, ME+NC achieved the greatest anti-edema endpoints, and in yeast-induced pyrexia, it produced the largest $AUC_{\Delta T}$ and maximum ΔT reduction. Collectively, these model-concordant results support the biological plausibility that a dose-sparing interaction observed *in vitro* can

translate into multi-symptom efficacy *in vivo* under standardized testing conditions.

Mechanistic biomarker patterns provide a plausible bridge between CI/DRI-defined synergy and *in vivo* phenotypes. Pro-inflammatory cytokines and oxidative mediators contribute to sensitization and amplification of pain signaling, and ROS can interact with cytokine programs to maintain pronociceptive states.[27] In macrophage-/microglia-linked inflammatory settings, coordinated suppression of iNOS/NO, COX-2/PGE_2, cytokines, and ROS is commonly interpreted as convergence on shared inflammatory-redox nodes.[28] Consistent with this framework, ME+NC produced the largest reductions in pro-inflammatory cytokines and COX-2/iNOS alongside the most favorable redox profile relative to vehicle and monotherapies. While these associations are not causal, they align with a shared mediator network capable of concurrently influencing nociception, edema, and fever.[29]

Safety readouts contextualize the dose-sparing claim. No adverse trends were evident in body-weight trajectory, liver/kidney biomarkers, or the representative histology presented, supporting the interpretation that the observed efficacy gains were not accompanied by overt toxicity signals within the 14-day observation window. However, these findings should be interpreted as evidence of short-term tolerability under the study conditions rather than as a comprehensive toxicological evaluation.

Several limitations and next steps remain. First, synergy was quantified *in vitro* and supported phenotypically *in vivo*; formal *in vivo* CI estimation would benefit from broader dose grids and explicit fixed-ratio designs within each *in vivo* model. Second, the study does not yet establish an exposure-response linkage demonstrating improved curcumin exposure from NC *in vivo*; model-informed PK/PD approaches are widely used in drug delivery to connect exposure and response and guide optimization.[30] Third, LC-MS/MS-based bioanalysis is a standard tool to trace nano drug-delivery fate *in vivo* and would enable pharmacokinetic profiling to support ratio optimization and exposure-response modeling.[31] Finally, the current models are acute; longer-term inflammatory pain and chronic inflammation paradigms will be required to evaluate durability and safety margins. In addition, formal *in vivo* ED50 estimation was not performed, as the present design used single *in vivo* doses aligned to the *in vitro* Dm-derived ratio; future studies employing multiple dose levels per agent would enable *in vivo* dose-response modeling and ED50 determination.

5. CONCLUSION

A QC-anchored *M. malabathricum* leaf extract-nanocurcumin combination demonstrated quantifiable Chou-Talalay synergism with practical dose-sparing for both components (CI < 1; DRI 2-3-fold at Fa 0.50-0.90) in an inflammatory macrophage assay. This interaction translated into consistent *in vivo* efficacy across models of analgesia, acute inflammation, and pyrexia, with positive-control benchmarking supporting assay sensitivity and interpretable effect magnitude. Biomarker profiling supported multi-target inflammatory-redox network modulation, and the 14-day tolerability readouts indicated no overt toxicity signals in the measured endpoints under the study conditions. Overall, ME+NC represents a promising dose-sparing, multi-symptom candidate warranting ratio optimization, PK/PD linkage, and validation in longer-term disease models.

6. ACKNOWLEDGEMENTS

The authors gratefully acknowledge the institutional and departmental support that enabled this study. The authors also thank the technical staff for assistance with chromatographic characterization and *in vivo* experimentation.

Author contribution

Thi Phuong Nhung Tran: Conceptualization, Methodology, Investigation, Formal analysis, Data curation, Supervision, Project administration, Writing – original draft, Writing – review and editing.
Co-authors (Hong Quan Bui, Huyen Trang Luu, Ngoc Thuan Nguyen, Thi Truc Ly Le, Hoa Hong Chau Truong): Data curation, Investigation. All authors read and approved the final manuscript.

Funding

The authors declare that no funds, grants, or other support were received during the preparation of this manuscript.

Conflict of interest

The authors declare that they have no conflict of interest.

Ethics approval

All animal procedures were conducted in accordance with institutional guidelines for the care and use of laboratory animals and were approved by the Institute's Animal Ethics Committee, Approval No. 206DH/DHNN.

Article info:

Received January 17, 2026
Received in revised form -
Accepted April 6, 2026

REFERENCES

1. Tran TPN, Vu TH, Nguyen TN. Mechanistic and pharmacological evaluation of *Cassia rhombifolia* fruit extract in murine models of pain, fever, and acute inflammation.

Science and Technology Indonesia. 2026;11(1):1-12. doi:10.26554/sti.2026.11.1.366-377.
2. Tran TPN, Le PTQ, Dang TKT. Ethanol extract from *Argyreia acuta* Lour. leaves exhibit analgesic, antipyretic, and anti-inflammatory effects in mouse models. BioTechnologia. 2025;106(2):1-14. doi:10.5114/bta/204527.
3. Kim ME, Lee JS. Advances in the regulation of inflammatory mediators in nitric oxide synthase: implications for disease modulation and therapeutic approaches. Int. J. Mol. Sci. 2025;26(3):1204. doi:10.3390/ijms26031204.
4. Sun W, Shi S, Liao S, Zhai M. Chikungunya fever: pathogenesis and mechanisms underlying pain symptoms. Front. Immunol. 2025;16:1679385. doi:10.3389/fimmu.2025.1679385.
5. Zakaria ZA, Raden Mohd Nor RNS, Kumar GH, Abdul Ghani ZDF, Sulaiman MR, Rathna Devi G, et al. Antinociceptive, anti-inflammatory, and antipyretic properties of *Melastoma malabathricum* leaves aqueous extract in experimental animals. Can. J. Physiol. Pharmacol. 2006;84(12):1291-9. doi:10.1139/y06-083.
6. Lestari OA, Palupi NS, Setiyono A, Kusnandar F, Yuliana ND. LC-MS metabolomics and molecular docking approaches to identify antihyperglycemic and antioxidant compounds from *Melastoma malabathricum* L. leaf. Saudi J. Biol. Sci. 2024;31(8):104047. doi:10.1016/j.sjbs.2024.104047.
7. Ipar VS, Dsouza A, Devarajan PV. Enhancing curcumin oral bioavailability through nanoformulations. Eur. J. Drug Metab. Pharmacokinet. 2019;44(4):459-80. doi:10.1007/s13318-019-00545-z.
8. Karthikeyan A, Senthil N, Min T. Nanocurcumin: a promising candidate for therapeutic applications. Front. Pharmacol. 2020;11:487. doi:10.3389/fphar.2020.00487.
9. Percie du Sert N, Hurst V, Ahluwalia A, Alam S, Avey MT, Baker M, et al. The ARRIVE guidelines 2.0: Updated guidelines for reporting animal research. J. Cereb. Blood Flow Metab. 2020;40(9):1769-1777. doi:10.1177/0271678X20943823.
10. Huang W, Percie du Sert N, Vollert J, Rice ASC. General principles of preclinical study design. Handb. Exp. Pharmacol. 2020;257:55-69. doi:10.1007/164_2019_277.
11. Tran TPN, Nguyen T-T, Tran G-B. Anti-arthritis effect of ethanol extract of Sacha inchi *(Plukenetia volubilis* L.) leaves against complete Freund's adjuvant-induced arthritis model in mice. Trop. Life Sci. Res. 2023;34(3):237-57. doi:10.21315/tlsr2023.34.3.13.
12. Nhung TTP. Correlation-driven analysis of synergistic effects of dual medicinal mushroom extracts in a DMBA-induced murine breast cancer model. Trop. J. Nat. Prod. Res. 2025;9(8):3496-504. doi:10.26538/tjnpr/v9i8.7.
13. Zhang H, Zhang L, Gao F, Yang S, Deng Q, Shi K, et al. Purification, composition, and anti-inflammatory activity of polyphenols from sweet potato stems and leaves. Foods. 2025;14(16):2903. doi:10.3390/foods14162903.
14. Angsusing J, Samee W, Mangmool S, Dortae U, Keawthip P, Mahasirimongkol S, et al. Antioxidant and anti-inflammatory activities of Thai traditional hand and foot soaking formula and its bioactive compounds. Pharmaceutics. 2025;17(7):907. doi:10.3390/pharmaceutics17070907.
15. Chou T-C. Drug combination studies and their synergy quantification using the Chou-Talalay method. Cancer Res. 2010;70(2):440-6. doi:10.1158/0008-5472.CAN-09-1947.
16. Nhung TTP, Quoc LPT. *In vivo* analgesic, antipyretic, and anti-inflammatory potential of ethanol extract *from Plukenetia volubilis* Linneo leaves in mice. Int J Agric Technol. 2024;20(5):2035-54.
17. Javaid F, Gul H, Ullah Khan K, Basit A. Behavioral assessment to evaluate the analgesic and anti-inflammatory effects of Fagonia bruguieri var. laxa Boiss by targeting pro-inflammatory cytokines and prostaglandin pathways. J Ethnopharmacol. 2025;342:119382. doi:10.1016/j.jep.2025.119382.
18. Mbugua CK, Mwonjoria JK, Njagi ENM. Anti-inflammatory, antinociceptive, and antipyretic potential of methanol extract of *Strychnos henningsii* in animal models. Int J Inflam. 2025;2025:3982255. doi:10.1155/ijin/3982255.
19. Aguilar Díaz de León J, Borges CR. Evaluation of oxidative stress in biological samples using the thiobarbituric acid reactive substances assay. J Vis Exp. 2020;(159):61122. doi:10.3791/61122.
20. Quan BH, Nhung TTP. Dose-response evaluation of *Blumea balsamifera* leaf ethanol extract in acute and subchronic toxicity models in mice for sustainable application. Trop J Nat Prod Res. 2025;9(9):4250-9. doi:10.26538/tjnpr/v9i9.22.
21. Noviana E, Indrayanto G, Rohman A. Advances in fingerprint analysis for standardization and quality control of herbal medicines. Front Pharmacol. 2022;13:853023. doi:10.3389/fphar.2022.853023.
22. Aslam B, Hussain A, Bari MU, Faisal MN, Zia ud Din Sindhu, Alonaizan R, et al. Anti-pyretic, analgesic, and anti-inflammatory activities of meloxicam and curcumin co-encapsulated PLGA nanoparticles in acute experimental models. Metabolites. 2023;13(8):935. doi:10.3390/metabo13080935.
23. Zahra N, Fatima S, Nazir A, Farrukh SY, Anwer A, Sarwar A, et al. *In vivo* and *in silico* analysis of anti-inflammatory, antipyretic, and analgesic activity of methanolic extract of Nigella sativa. J Mol Histol. 2025;56(2):118. doi:10.1007/s10735-025-10399-2.
24. Najafi F, Farrokhzad N, Ghaemi A, Azizi Khezri D, Hajiabbas MA, Khanizadeh A, et al. Advancement in nanocarrier-mediated delivery of herbal bioactives: from bench to bedside. Nat Prod Bioprospect. 2025;15(1):69. doi:10.1007/s13659-025-00550-7.
25. Liu Y, An D, Meng X, Deng S, Liu G. Zein-based nanocarriers: Advances in oral drug delivery. Pharmaceutics. 2025;17(7):944. doi:10.3390/pharmaceutics17070944.
26. Kifer D, Jakšić D, Šegvić Klarić M. Assessing the effect of mycotoxin combinations: Which mathematical model is (the most) appropriate? Toxins (Basel). 2020;12(3):153. doi:10.3390/toxins12030153.
27. Silva CEA, Guimarães RM, Cunha TM. Sensory neuron-associated macrophages as novel modulators of neuropathic pain. Pain Rep. 2021;6(1):e873. doi:10.1097/PR9.0000000000000873.
28. Lo J, Liu C-C, Li Y-S, Lee P-Y, Liu P-L, Wu P-C, et al. Punicalagin attenuates LPS-induced inflammation and ROS production in microglia by inhibiting the MAPK/NF-κB signaling pathway and NLRP3 inflammasome activation. J Inflamm Res. 2022;15:5347-59. doi:10.2147/JIR.S372773.
29. Tong S-H, Liu D-L, Liao P, Zhang S-Y, Zhou J, Zong Y, et al. Emerging role of macrophages in neuropathic pain. J Orthop Translat. 2025;51:227-41. doi:10.1016/j.jot.2025.01.016.
30. Zou H, Banerjee P, Leung SSY, Yan X. Application of pharmacokinetic-pharmacodynamic modeling in drug delivery: development and challenges. Front Pharmacol. 2020;11:997. doi:10.3389/fphar.2020.00997.
31. Wang T, Zhang D, Sun D, Gu J. Current status of *in vivo* bioanalysis of nano drug delivery systems. J Pharm Anal. 2020;10(3):221-32. doi:10.1016/j.jpha.2020.05.002.